Perspective: Coherent Raman scattering microscopy, the future is bright

Chi Zhang, and Ji-Xin Cheng

Citation: APL Photonics **3**, 090901 (2018); doi: 10.1063/1.5040101
View online: https://doi.org/10.1063/1.5040101
View Table of Contents: http://aip.scitation.org/toc/app/3/9
Published by the American Institute of Physics

Perspective: Coherent Raman scattering microscopy, the future is bright

Chi Zhang and Ji-Xin Cheng[a]
Department of Biomedical Engineering, Department of Electrical and Computer Engineering, Boston University, Boston, Massachusetts 02215, USA

(Received 14 May 2018; accepted 27 June 2018; published online 25 July 2018)

Chemical imaging offers critical information to understand the fundamentals in biology and to assist clinical diagnostics. Label-free chemical imaging piques a general interest since it avoids the use of bio-perturbing molecular labels and holds promises to characterize human tissue *in vivo*. Coherent Raman scattering (CRS), which utilizes lasers to excite the vibrations of molecules, renders new modalities to map chemicals in living samples without the need of labeling and provides significantly improved speed, resolution, and sensitivity compared to spontaneous Raman scattering. Although microscopy systems based on CRS have seen rapid development in the past two decades, remaining challenges, which emerge in diverse aspects, start to impede the continuous advancement of the field. In this perspective, we review the history of CRS microscopy, scrutinize the pros and cons of different modalities, and discuss the current challenges and possible future directions of the field. Infiltration of conceptual and technological ideals from other fields will promote CRS microscopy towards a versatile tool for basic science and medical research.
https://doi.org/10.1063/1.5040101

I. HISTORY AND EARLY DEVELOPMENT

Raman scattering, discovered by Raman and co-workers in the 1920s,[1] not only convincingly proved the quantum nature of light but also provided scientists with an outstanding tool to elucidate the structures of molecules using visible light. First, the inelastic scattered Raman photons carry information of molecular vibrations which are, in terms of energy, in the mid-infrared (IR) range. The switch from mid-IR to visible beams circumvents the overwhelming absorption from ubiquitous water molecules, thus having unprecedented value for applications in biology and medical sciences. Second, with Raman spectroscopy, chemical labeling is no longer a prerequisite for obtaining chemical information in samples. These aspects allow biological samples to stay hydrogenated, alive, and unperturbed for characterization, which are critical to accurately understand biofunctions.

Notwithstanding the advantages, spontaneous Raman scattering is a "very feeble secondary radiation."[2] The Raman scattering cross section is typically on the level of 10^{-30} cm^2 per molecule, which is about 10^{11} times smaller than the IR absorption cross section. The low efficiency in spontaneous Raman scattering results in long signal integration time and slow spectral acquisition speed. When used for imaging, such a low speed prevents practical mapping of highly dynamic living samples. Since the advent of lasers, nonlinear optical processes were made practical and multiple processes were used to boost the signal of Raman scattering. The major approaches include synchronizing the local oscillators by coherent anti-Stokes Raman scattering (CARS) and enhancing the Raman quantum efficiency by stimulated Raman scattering (SRS). Microscopic systems based on both CARS and SRS have been extensively developed for various biological applications.

CARS and SRS typically involve two input laser fields, a pump laser at ω_p, and a Stokes laser at ω_s, to interact with a sample. In a molecular point of view, the oscillation of electron clouds can be

[a]jxcheng@bu.edu

driven efficiently by the beat frequency of the two lasers when $\omega_p - \omega_s$ approaches the vibrational resonance frequency ω_v. This effectively couples the photon energy to the molecular vibrations while conserving the total number of photons. Consequently, the photons annihilated in the pump beam are converted to those in the Stokes beam. On the other hand, the coherently oscillating electron motion alters the refractive index of the sample, which can be probed by another beam, e.g., by the same pump beam to generate a new (anti-Stokes) frequency at $\omega_p + \omega_v$. The enhanced quantum efficiency in the photon-vibration energy transfer gives rise to SRS, and the coherent buildup of the photon-perturbed vibrations is detected by CARS. Quantum mechanical descriptions of CARS and SRS can be found in other materials.[3,4]

Notably, the first observation of CARS, which can be dated back to 1965, was reported by researchers at the Ford Motor Company, a company dedicated to produce cars;[5] yet, the official name of "CARS" was not granted until 10 years later by Begley and co-workers.[6] Over the years, CARS spectroscopy has been and remains as a powerful tool for combustion diagnostics.[7–10] Duncan and co-workers in 1982 reported the first CARS microscope using a non-collinear beam geometry.[11] In 1999, Xie and co-workers reported a CARS microscope based on synchronized high-repetition-rate femtosecond pulses using a collinear beam and tight-focusing geometry.[12] This work triggered the development of modern CARS microscopy. Since then, CARS signal generated in the tight-focusing condition has been systematically studied.[13] Picosecond-pulse-based laser-scanning CARS microscopy was developed for high-speed imaging of biological samples,[13] and the speed of CARS imaging has reached video-rate in 2005.[14] CARS signal is usually detected by a highly sensitive photomultiplier tube (PMT), an avalanche photodiode, or a charge-coupled device (CCD). Theoretically, a CARS spectrum contains the same information as the corresponding spectrum from spontaneous Raman scattering. However, CARS signal is usually companied by a strong nonresonant background which could distort or even overwhelm the vibrational peaks. Multiple strategies, including polarization-sensitive detection,[15] epi-detection,[16] frequency modulation,[17] nonlinear interferometric vibrational imaging,[18] and spectral unmixing[19] were used to suppress or separate the nonresonant background and to extract pure Raman responses from CARS spectra.

The SRS phenomenon was discovered in 1960, even earlier than the first observation of CARS.[20] SRS was initially utilized as a spectroscopic technology.[21] In 2007, Ploetz *et al.* reported a broadband SRS microscope based on a high-energy low-repetition-rate laser.[22] In the following year, Xie and co-workers reported a high-speed single-frequency SRS microscope pumped by a laser with high-repetition rate.[23] In this work, the SRS signal was measured through modulation-transferred laser intensity from the Stokes beam to the pump beam.[23] In the meantime, several other groups reported their development of SRS microscopy.[24–26] The detection of SRS signal usually requires a silicon photodiode and a lock-in amplifier.[23] Slipchenko *et al.* reported a lock-in-free SRS detecting scheme based on a tuned-amplifier (TAMP).[27]

CARS and SRS imaging can be implemented on the same microscope with some modifications.[28] The favor of CARS or SRS is usually dependent on specific applications. Compared to CARS, the SRS signal does not contain the nonresonant background and can be detected under ambient light.[29] In addition, unlike the CARS signal which is quadratically proportional to the number of molecules probed, the SRS signal has a linear dependence on the molecular number density, reducing the complexity in quantitative analysis. On the other hand, SRS is not completely background-free. Cross phase modulation, transient-absorption, or photo-thermal effects can interfere with the SRS signal and complicate the image.[30] Instead, the measurement of CARS signal at a new anti-Stokes frequency sidesteps these pump-probe backgrounds. The nonresonant background in CARS has also been exploited to amplify the weak resonant signal of interest.[31] In addition, according to phase matching, CARS can be generated towards the epi-direction,[13] making it intrinsically favorable for *in vivo* imaging.

II. MOST RECENT TECHNICAL INNOVATIONS AND ENABLING APPLICATIONS

A. From single-color to hyperspectral CRS microscopy

Early CARS and SRS microscopes utilized narrowband laser beams to excite a single Raman transition.[15,23] Such a scheme allowed high-speed imaging of known compositions such as lipid

bodies[32] and myelin sheaths,[33] but it cannot discriminate molecules having overlapped Raman bands. Multi-color imaging improved the Coherent Raman scattering (CRS) selectivity by simultaneous exciting several Raman bands through parallel signal detection.[34] A fast tunable optical parametric oscillator was also deployed for three-color SRS imaging.[35] He *et al.* reported a rapid two-color SRS microscope using engineered pulse profile and dual-phase SRS detection by a single lock-in amplifier.[36] Combining with strip-mosaicing, this method has been used for rapid label-free histology of brain.[37] Multi-color SRS imaging has shown the capacity to produce label-free digital histology imaging similar to the standard hematoxylin and eosin (H&E) stain, and to image lipid, protein, and DNA in living cells and intact tissue.[38–40]

Hyperspectral CRS microscopy provides more informative spectral profile at each image pixel. Hyperspectral CARS imaging has been achieved via wavelength sweeping, spectral focusing, and multiplexing. Wavelength sweeping uses two narrowband (picosecond) laser beams and tunes the frequency of one of the beams continuously over a range while collecting an image at each step [Fig. 1(a)].[14] The image stack can then be used to build a spectrum at each pixel. In such a scheme, the signal from CARS is still detected by a single-channel detector such as a PMT. A second approach to obtain spectral information is by deploying two broadband (femtosecond) lasers beams and chirping the pulses to narrow down spectral frequency compositions for the time-domain overlap, which is usually known as the spectral-focusing scheme [Fig. 1(b)].[41,42] To acquire a spectrum using the spectral-focusing, a time-delay between the two pulses needs to be scanned, and a single-channel detector is used to collect the signal. Notably, the frame-by-frame image acquisition is inapplicable to image highly dynamic living samples since a movement from the sample during the frequency scan can distort CARS spectra. Multiplex CARS microscopy solves this problem by simultaneously exciting a broad range of Raman frequencies [Fig. 1(c)] and collecting a spectrum using an array detector.

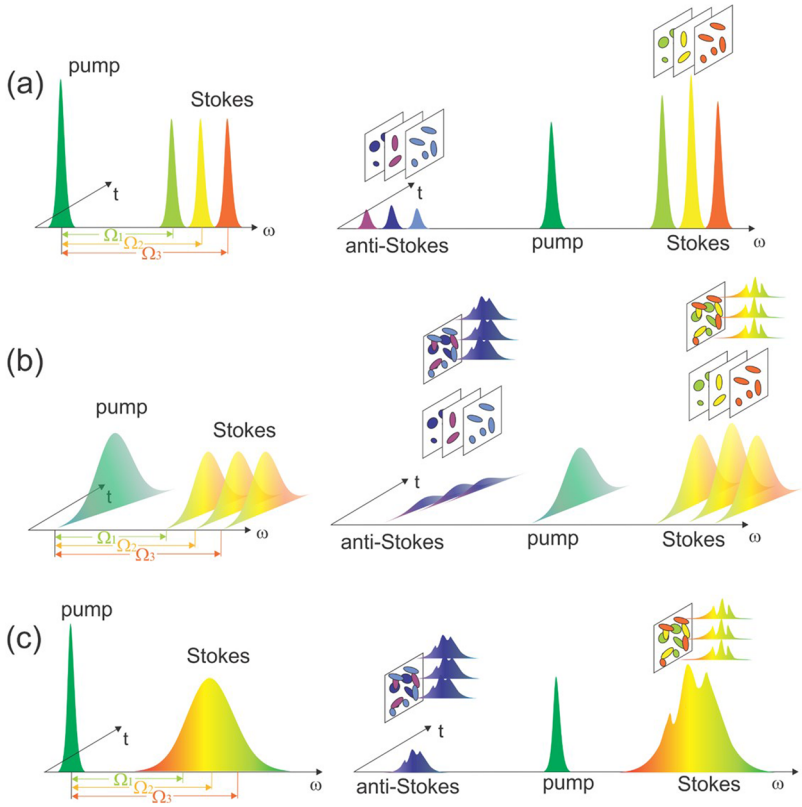

FIG. 1. Methods for hyperspectral CRS microscopy. (a) CRS microscopy based on frequency tuning of narrowband pump and Stokes beams. (b) CRS microscopy based on spectral focusing of broadband pump and Stokes beams. (c) Multiplex CRS microscopy using a narrowband pump and a broadband Stokes. Commonly used image collection schemes are demonstrated as frame-by-frame or spectrum-by-spectrum.

Multiplex CARS was first implemented by using a narrowband pump beam and a broadband Stokes beam.[43,44] Broadband laser sources offer flexibility to implement high-speed hyperspectral CARS imaging.[45–47] Ultra-broadband supercontinuum light source provides a convenient and powerful way to implement broadband CARS.[48–50] By intra-band excitation, Cicerone and co-workers demonstrated broadband CARS imaging over a 3500 cm^{-1} spectra range at a speed of 3.5 ms per pixel.[51]

Hyperspectral SRS microscopy has been achieved in the frame-by-frame mode by wavelength tuning of narrowband laser pulses [Fig. 1(a)] which are obtained through pulse-shaping of femtosecond pulses.[52,53] Using such a scheme, an imaging speed of 30 frames per second covering a spectral window of 300 cm^{-1} was reported by Ozeki *et al.*[52] Besides, spectral-focusing was also widely adopted for hyperspectral SRS microscopy [Fig. 1(b)].[54,55] He *et al.* used a galvo mirror and a grating to rapidly scan the optical delay line and obtained an SRS spectrum in 500 μs.[56] High-speed delay line tuning using a resonant mirror can acquire an SRS spectrum in 42 μs.[57] Harnessing the low-rank property of hyperspectral images, Lin *et al.* showed that random sub-sampling in the frequency-spatial domain can reconstruct the entire hyperspectral image stack without information loss through matrix completion.[58] These high-speed tuning schemes reduce spectral distortion for slow sample movement but are still problematic for fast moving samples. Multiplex SRS microscopy [Fig. 1(c)] provides an ultimate solution for the problem. The parallel detection of SRS signals at different Raman shifts can be achieved by a complementary metal oxide semiconductor (CMOS) array[59] or a multi-channel lock-in amplifier,[60] both having a detection sensitivity of 10^{-4} *dI/I* modulation depth. Cheng and co-workers invented a 16-channel TAMP array to extract SRS signals, which allowed for acquisition of an SRS spectrum within 32 μs with a 10^{-6} *dI/I* detection limit.[61] Zhang *et al.* reported an acquisition of an SRS spectrum in 5 μs by a 32-channel TAMP array, which offers a new way for high-throughput single-cell chemical analysis in a flow setting.[62] Coding optical frequencies with different modulation frequencies and extracting Raman responses from Fourier transform provides an elegant way for high-speed hyperspectral SRS imaging.[63] This approach only requires a single photodiode which can be placed close to the sample, thus suitable for collecting highly scattered photons from a thick biological specimen.

Advanced data analysis schemes were adopted to convert the hyperspectral images to chemical maps. Multivariate curve resolution analysis[53,64] and singular value decomposition analysis[65] was applied to segment images based on hyperspectral CRS data. Based on the broadband CARS, the Borri group and the Langbein group developed a "Factorization into Susceptibilities and Concentrations of Chemical Components" (FSC^3) method to quantitatively analyze lipid content in single cells.[66–68] This allowed for chemical profiling of individual lipid droplets and single cells to understand lipid uptake.[69] In addition, sparse sampling was applied with the FSC^3 method to reduce the image acquisition time by a factor of 25.[70] Bessel-beam-based excitation scheme further enabled high-speed metabolic profiling of lipids in response to drug treatment.[71] Maximum entropy method was first used to retrieve Raman spectral information from broadband CARS spectra, reported by the Müller group[72,73] and the Kano group.[74] The Cicerone group reported a broadband CARS microscope capable of covering the entire biologically relevant Raman window from 500 cm^{-1} to 3500 cm^{-1} and extract the broadband CARS spectra through time-domain Kramers-Kronig transform.[51]

The spectral information in imaging has enabled discoveries of new biology. For example, using hyperspectral SRS microscopy, the Xie group found intracellular enrichment of tyrosine-kinase inhibitor drugs in lysosomes, which is responsible for reduced efficacy of these drugs.[75] By coupling single-color SRS with spontaneous Raman on the same platform, the Cheng group discovered cholesteryl-ester accumulation in prostate cancer cells, which was found related to cancer aggressiveness.[76] Comparing SRS spectra of lipid droplets, Li *et al.* found increased lipid desaturation as new metabolic marker for ovarian cancer stem cells.[77] This research offers a new way to identify cancer stem cells without labeling, and new strategies to effectively remove cancer stem cells targeting their metabolism.[77]

B. From milli-molar sensitivity to single molecule detection

Regarding the detection sensitivity, the selection of CARS or SRS depends on specific conditions. Theoretically, CARS is more sensitive when the sample concentration is high due to the quadratic

dependence of signal with respect to the molecular number density. For more dilute samples, SRS is preferable because of a less decrease in signal intensity and an absence of the nonresonant background. However, for sample systems having low energy in electronic transitions, two photon absorption or pump probe effects can complicate the SRS signal detection. Although the CARS nonresonant background is also enhanced in such conditions, the heterodyne amplification can actually improve the CARS signal, potentially allowing for higher sensitivity.[31,78] To separate the resonant signal from the nonresonant background, maximum entropy method[72,73] or the Kramers-Kronig-transform-based image processing algorithm is usually required.[19] CARS was reported to have a sensitivity of detecting 70 millimolar (mM) dimethyl sulfoxide (DMSO) with a pixel dwell time of 10 μs,[79] corresponding to about 2.5×10^5 oscillators in a 0.06 fl focal volume. The sensitivity of SRS is on the level of 21 mM DMSO with a pixel dwell time of 83 μs,[57] corresponding to about 7.7×10^4 oscillators in the same focal volume.

Advanced schemes have been developed to push the CRS detection limits. Through plasmonic enhancement of nanostructures [Figs. 2(a) and 2(b)], CARS was shown to detect single molecules for which the vibrational coherence detected in the far field shows phase fluctuations rather than pure dephasing (Fig. 2).[80] Utilizing an atomic tip for near-field detection, SRS-transition-induced changes in atomic forces can be measured at a near-single-molecule-level.[81,82] Such an approach can provide chemical imaging with a lateral resolution below 10 nm, approaching the single-molecule regime. Taking the advantage of a large cross section of CC triple bond, a detection limit of 31 micromolar (μM) phenyl-diyne cholesterol (i.e., 1800 molecules inside the focal volume) has been reached using spectrally focused femtosecond SRS microscopy.[83] Recently, the concept of pre-resonance Raman was used to enhance the signal of SRS. The Min group showed that careful detuning the excitation from

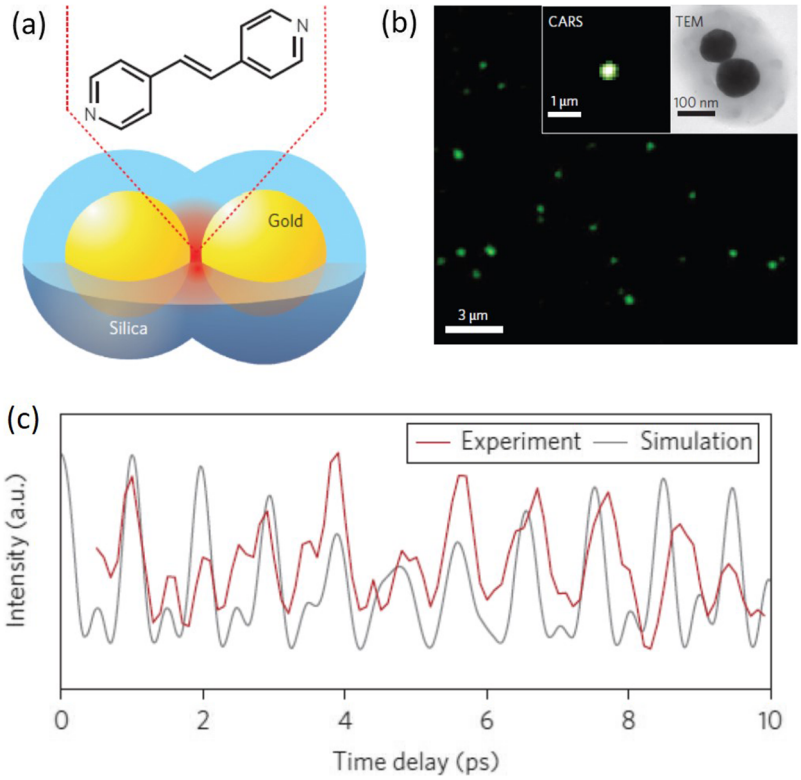

FIG. 2. CARS imaging of a single molecule. (a) A sketch of the dumbbell-shaped gold nanostructures with attached *trans*-1,2-bis-(4-pyridyl) ethylene molecules. (b) CARS image and isolated dumbbell nanostructures. Inset: CARS image of a single dumbbell structure and the corresponding transmission electron microscopy image. (c) Time-resolved CARS signal trace of a single structure showing distinct quantum beats (experimental and simulations curves). Adapted with permission from Yampolsky *et al.*, Nat. Photonics **8**(8), 650–656 (2014). Copyright 2014 Springer Nature.

the electronic resonance can retain both the Raman signal enhancement and the chemical selectivity.[84] A palette of 24 conjugated Raman probes with separable spectral peaks were created working in this pre-resonance condition, underscoring the potential for super-multiplex optical imaging.[84] The SRS imaging sensitivity can also be improved through data processing approaches. For example, Liao *et al.* reported a denoising algorithm via total variation minimization to reduce noises in both spatial and spectral domains for SRS imaging.[85]

C. From planar to volumetric imaging

The nonlinear nature of CRS brings sectioning capability to CRS microscopes. Although wide-field CARS was reported,[86–88] most CRS microscopes utilize tightly focused Gaussian beams for excitation and scan the collinearly combined beams by two-dimensional (2D) laser scanning [Fig. 3(a)], which can sample through a planar area of hundreds of micrometers across. Large-area mapping on the scale of centimeters can be achieved by stitching tens or hundreds of images. To measure a three-dimensional (3D) structure using such a scheme, axial scanning of the sample or the laser focus is required. This can be achieved by using a translational or a piezo scanning stage. Such a 3D imaging methodology is easy to implement but can be inefficient for sweeping through a large volume. In addition, the axial resolution is usually worse than the lateral resolution due to the shape of focused Gaussian beams.

Chen *et al.* reported an alternative method utilizing Bessel beam excitation for high-speed 3D SRS imaging.[89] The central lobe of a Bessel beam can maintain its focus over a long range, thus can be used to extend the depth of focus for SRS excitation. The SRS signal was generated along the extended focus and integrated as a single point. A 2D scanning of the Bessel beam over a 3D volume generates a projection image of the volume [Fig. 3(b)]. Such a method can provide high-speed quantitation of chemical information in a volume, at a price of losing the axial resolution. Deploying a tomographic approach, which collects projection images at different projection angles, the 3D information can be reconstructed using a filtered back projection algorithm [Fig. 3(c)].[89] In this way, the spatial resolution of the 3D image is identical in all directions [Fig. 3(d)]. Recently, Masia *et al.* reported Bessel-beam hyperspectral CARS microscopy combined with sparse sampling.[71] This new approach enabled high-throughput and high-content quantitation of lipid compositions in liver cells.[71]

D. Improved chemical specificity

Most chemical bonds measured in Raman spectroscopy are shared by many biomolecules. For example, the CH_2 bonds can be found in nearly all lipids and proteins. The CH_3 bonds can be found

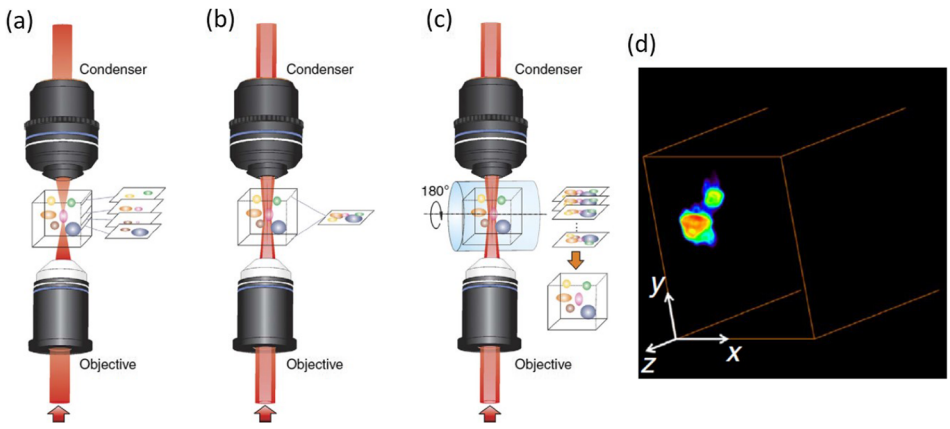

FIG. 3. Volumetric imaging modalities based on stimulated Raman projection (SRP). (a) Sectional imaging by the conventional Gaussian beam SRS microscopy. (b) SRP microscopic imaging based on Bessel beams. (c) SRP tomographic imaging based on Bessel beams. (d) Reconstructed 3D structure of lipid molecules in a 3T3-L1 adipose cell. Adapted with permission from Chen *et al.*, Nat. Commun. **8**, 15117 (2017). Copyright 2017 Springer Nature.

in almost all proteins and DNA molecules. Therefore, Raman essentially relies on the different combinations, or ratios, of chemical bonds to separate different biomolecules. Proteins are too complex to identify using this way. On the other hand, for the small molecules such as metabolites, their relatively simple structures provide a niche for Raman to have higher chemical specificity than fluorescence. For example, comparing Raman peak ratios, it is able to separate cholesteryl ester from triglyceride,[76] or differentiate lipids with different saturation levels.[77]

To improve the chemical specificity, a common way is through "Raman tags" or isotope labeling. Raman tags are usually small chemical bonds which are highly conjugated (such as alkyne, nitrile, or phenyl ring). These bonds have very strong Raman responses due to their susceptible electron clouds, generating large signals in CRS. More importantly, the Raman peaks of these tags are usually located in the vibrational "silent" range (1900-2600 cm^{-1}), which do not overlap or interfere with intrinsic molecular vibrations from biological samples. The Raman tags improved the chemical selectivity of CRS microscopy for imaging lipids, proteins, and DNA (Fig. 4).[83,90–93] Isotopic labeling, which can shift vibrational frequencies of chemical bonds, provides another way to selectively target molecules of interest.[90,94,95] In addition, Raman spectra are much narrower than fluorescence spectra, allowing more detection channels to be applied for multicolor imaging. The Min group developed a series of probes for Raman super-multiplexing through rational design of conjugation, isotope editing, and end-group variation.[84,96] Introducing a specific isotopic compound which does not exist inherently allows pulse-chase analyses to understand the function of the compound through CRS imaging. Commonly used isotopic labeling includes replacing the hydrogen with the deuterium,[97] or substituting the carbon-12 with the carbon-13,[98] both have minimum perturbation to biological functionality. With isotopic labeling, CRS was used to study synthesis of proteins and the conversion of lipids from glucose.[90,98]

Notably, the CRS signal is polarization dependent, offering information about molecular orientations. Usually, the strongest CRS signal is found when excitation fields most effectively polarize the chemical bonds. This indicates that if molecules have a net orientation on the lateral plane, polarization dependent CRS allows for elucidation of their orientations. Using such a method, orientation information of water molecules near a plasma membrane,[99] and the lipid molecules composing the membrane[100,101] were deduced from CARS images. Radically polarized or rotating-polarization CARS and SRS microscopes were developed relying on this concept to image molecular orientations.[102–104] Using circularly polarized light, SRS microscopy was shown to retrieve molecular symmetry of the sample.[105]

E. High-throughput single-cell analysis

Although the imaging speed of CRS microscopy can be as fast as fluorescence microscopy, only a few cells are usually measured in a single frame. To understand cells as a population, a large amount of measures are necessary. This requires a high-throughput scheme to probe single cells and to quantitate their cellular chemical compositions. In fluorescence, such a high-throughput analysis can be achieve through flow cytometry, which directs the cells to flow through the laser focus for rapid measurement. Flow cytometry based on spontaneous Raman scattering suffers from low speed due to the weak signal level. The throughput of spontaneous Raman flow cytometry is usually four orders of magnitudes lower than that of the fluorescence-based flow cytometry. CRS provides opportunities for the speed breakthrough. Microfluidic CARS flow cytometry was first demonstrated by the Cheng group for analyzing polymer particles and adipocytes at a throughput of tens of particles per second.[106] This first attempt for CARS flow cytometry only has a single spectral channel. Camp *et al.* developed a prototype for multiplex CARS flow cytometry using a supercontinuum source.[107] However, due to the low spectral output of CCDs, the speed of CARS flow cytometry is on the level of 4 mm/s.[108] Using the multiplex SRS scheme, Liao *et al.* demonstrated visualization of flowing cells and separation of different chemical compositions inside cells.[61] This was achieve by a lab-designed TAMP array having 16 spectral channels. In 2017, Zhang *et al.* demonstrated a prototypic multiplex SRS flow cytometer based on an upgraded photodiode array detector having 32 spectral channels.[62] This new device can acquire 200 000 SRS spectra in 1 s, corresponding to 5 μs per Raman spectrum [Figs. 5(a)–5(c)] and can analyze up to 11 000 particles per second [Figs. 5(d) and 5(e)].[62]

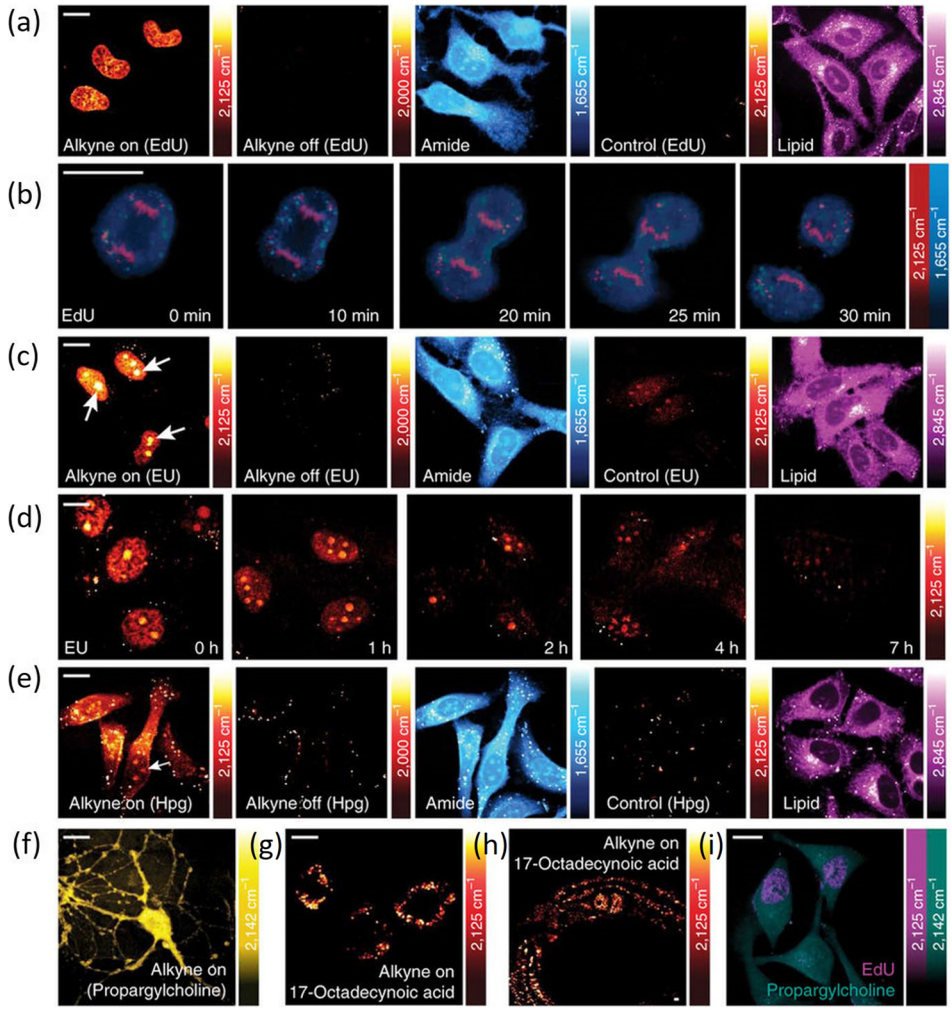

FIG. 4. Live SRS imaging of *de novo* synthesis of DNA, RNA, proteomes, phospholipids, and triglycerides by metabolic incorporation of alkyne-tagged small precursors. (a) Live HeLa cells incubated with 100 μM 5-ethynyl-2′-deoxyuridine (EdU) alone (alkyne on) and with 10 mM hydroxyurea (control). (b) Time-lapse images of a dividing cell incubated with 100 μM EdU. (c) Live HeLa cells incubated with 2 mM 5-ethynyl uridine (EU) alone (alkyne on) and with 200 nM actinomycin D (control). (d) Pulse-chase imaging of RNA turnover in HeLa cells incubated with 2 mM EU for 12 h followed by EU-free medium. (e) Live HeLa cells incubated with 2 mM l-homopropargylglycine alone (alkyne on) and with 2 mM methionine (control). (f) Live neurons incubated with 1 mM propargylcholine (alkyne on). (g) Live macrophages incubated with 400 μM 17-octadecynoic (17-ODYA) (alkyne on). (h) *C. elegans* fed with 17-ODYA (alkyne on). (i) Dual-color images of simultaneous EdU (2125 cm^{-1}, magenta) and propargylcholine (2142 cm^{-1}, green) incorporation. Reprinted with permission from Wei *et al.*, Nat. Methods **11**(4), 410–412 (2014). Copyright 2014 Springer Nature.

F. Rapid label-free histology

In conventional histology, the excised tissue needs to be fixed or frozen, sliced and stained with H&E before analyzed under a microscope. Although the H&E stain provides a gold standard for pathological diagnosis, it is not performed *in vivo* and requires tissue sectioning and therefore is time consuming. CRS microscopy offers unique contrast to generate histology-like images for diagnostics, which shows potential for next generation rapid label-free histology.

Evans *et al.* first applied single-color CARS to image the whole mouse brain *ex vivo* for label-free pathology purposes.[109] Laser was tuned to excite lipid methylene stretching band at ~2850 cm^{-1}. Lighting up lipid distributions in brain also allows for stain-free pathological analysis of brain tumor.[110] However, such a lipid-only approach offers less information for accurate diagnosis. Multiplex CARS imaging gives more chemical selectivity, which would potentially improve

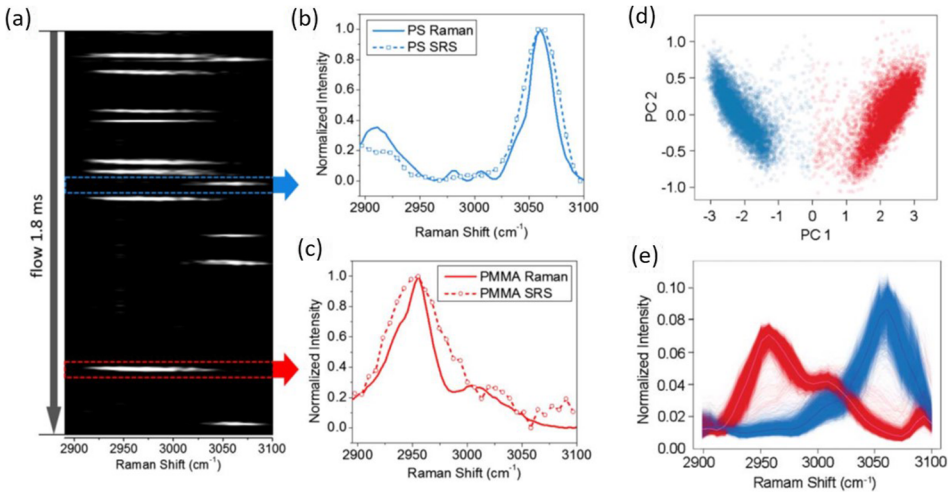

FIG. 5. High-speed single-particle analysis by multichannel SRS flow cytometry. (a) In a spectrum-time window recorded in 1.8 ms, 8 PMMA beads (peak centered at 2955 cm^{-1}) and 5 PS beads (peak centered at 3060 cm^{-1}) were detected. (b) SRS (dashed line with open squares) and spontaneous Raman (solid line) spectra of polystyrene beads. (c) SRS (dashed line with open circles) and spontaneous Raman (solid line) spectra of PMMA beads. (d) Compositional principal component analysis result of SRS spectra collected from a mixture of PMMA and PS beads. The spectra of ~8000 particles were collected in 1 s. (e) Corresponding SRS spectra. Adapted with permission from Zhang *et al.*, Optica **4**(1), 103–109 (2017). Copyright 2017 Optical Society of America.

pathological decision making.[111] Several issues remain in CARS-based histopathology. First, strong nonresonant background could distort and bury the resonant Raman spectra. Second, the nonlinear signal-concentration dependence in CARS complicates the quantitative analysis of brain tissue. Consequently, SRS imaging is becoming a more appealing tool for brain imaging. To provide histologic images similar to H&E stain, two-color contrast is needed. In SRS, such a contrast can be obtained from lipid and protein contents measured by CH_2 and CH_3 vibrations. Ji *et al.* reported two-color SRS imaging of brain tissues and showed that lipid/protein contents can offer key histological information to identify brain tumor and delineate tumor margin.[112,113] Two-color SRS imaging shows similar resolution and contrasts to those obtained from conventional H&E stain, but avoids tissue fixation, sectioning, and staining.[39] Lu *et al.* profiled 41 brain tumor specimens harvested from 12 patients using two-color SRS imaging and correlated the data with clinical gold standard histopathology for over 4000 field of view.[40] Essential diagnostic hallmarks for glioma classification have been identified from the SRS images.[40] Rapid intraoperative histology of unprocessed surgical brain tissue was reported by using a fiber-laser-based two-color SRS imaging platform developed for clinical settings.[114]

G. From bulk lasers to fiber lasers

The excitation of CRS microscopy requires two input lasers, usually in the visible or near-IR range. The most widely used laser source for CRS microscopy is crystal-based mode-locked bulk lasers, generating picosecond or femtosecond pulses. Frequency conversion systems such as an optical parametric oscillator (OPO) or supercontinuum are usually used in combination with the laser source to cover a broad range of Raman transitions. These bulk lasers are usually costly, bulky, and have strict environmental requirements. Fiber lasers, which are more cost-effective, compact, and robust, have been applied to CRS microscopy.[45,115–119] Compared to the crystal-based OPO, fiber-based frequency conversion systems have higher intensity noise in the MHz range. This noise does not affect the signal-to-noise-ratio in CARS but is problematic for SRS which typically requires modulation and demodulation of laser intensity at the MHz range. The balance-detection scheme effectively suppressed the noise for SRS microscopy.[120] Using this scheme, Orringer *et al.* recently demonstrated the first application of SRS histopathology using a portable fiber-laser-based SRS

microscope to analyze unprocessed specimens from 101 neurosurgical patients,[114] highlighting the potential of CRS microscopy in clinical translation.

III. REMAINING CHALLENGES AND POSSIBLE SOLUTIONS

With continuous efforts in the past two decades, CRS microscopy has gradually become mature and has infiltrated into many fields in biological, material, and medical sciences. Technological advancements have shaped CRS microscopy with higher sensitivity, higher imaging speed, and higher chemical selectivity. CRS microscopes are becoming robust and user-friendly tools available for scientists in non-optic fields. Nonetheless, challenges still remain for CRS microscopy to improve its impact and popularity in fundamental science and clinical translation.

A. Call for higher detection sensitivity

The major bottleneck of CRS microscopy is still the limited detection sensitivity. Any further improvement in the spatial-resolution, imaging speed, or imaging depth requires a boost in CRS sensitivity. Although single-molecule CARS and SRS spectroscopies have been reported,[80,81] such a sensitivity was achieve at specific hot spots between nanoparticles with specially designed geometry or at the tip used in an atomic force microscope, both non-applicable to study molecules in a living cell. Practically, label-free CRS microscopes have a sensitivity on the level of millimolars to micromolars, depending on the molecules under investigation. Such a sensitivity is not sufficient for mapping many important biomolecules such as neurotransmitters. Pre-resonance SRS imaging reached a sensitivity of nanomolars, however, relying on special Raman tags.[84] How to further improve the sensitivity of CRS microscopy is still an open question. For CARS, the coherent signal buildup slumps quadratically as the number of molecules decreases. Luckily, CARS signal from a small number of molecules can be enhanced through heterodyne amplification by the strong nonresonant signal from the surrounding media. To utilize such a local field enhancement, sophisticated spectral unmixing methods to separate resonant and nonresonant signals are required. For SRS, although its signal level is usually much stronger than CARS and is linearly linked to sample concentration, direct detection of laser beams produces high-level quantum noise, so-called shot noise. Eliminating the quantum noise in far field seems to be a mission impossible, but once achieved, might reshape the field. Another "thinking-outside-the-box" approach is to measure the refractive index changes induced by infrared absorption, which has a much larger cross section than Raman scattering.[121] Recently, Traverso *et al.* showed that mid-infrared two-photon resonance can enhance the CARS signal and reduce the nonresonant background, which could potentially improve the sensitivity of CRS microscopy.[122]

B. Call for deeper penetration

Similar to other nonlinear optical imaging modalities, CRS microscopy usually requires tightly focused laser beams to maximize the energy density for signal generation. CRS signal decreases drastically as the tight-focusing condition relaxes, offering the technology inherent sectioning capability while reducing its penetration depth. In general, CRS microscopy has much shallower imaging depth compared to modalities that do not require laser focusing, such as diffuse optical tomography or photoacoustic tomography. However, the tradeoff of imaging depth offers higher spatial resolution. Several approaches can potentially improve the imaging depth of CRS microscopy. The first method is purely optical, by introducing adaptive optics which could optimize wave fronts of input lasers to enhance the focusing condition in the deep tissue. This method has been applied to fluorescence microscopy[123] but has not been achieved for CRS largely due to the challenge to optimize wave fronts of both pump and Stokes beams using one adaptive optical device. The second possible way is to clear the tissue to reduce photon scattering caused by refractive index mismatch in biological samples.[124] Conventional tissue clearing methods alter the tissue content by removing lipid contents. A tissue clearance method to maintain the lipid composition is a more desired way for CRS microscopy. A third way is to use long wavelength excitation. Current CRS microscopes usually utilize near-IR beams for excitation. Shifting the excitation wavelength to even longer wavelengths is expected to further improve the imaging depth. Last but not least, several groups showed improved imaging depth

using engineered laser beams such as Bessel beams, for linear and nonlinear microscopies.[125–127] These engineered beams, which could bypass the scattering objects on surfaces, might allow CRS microscopy to see deeper.

C. Super-resolution CRS microscopy

CRS microscopy provides diffraction-limited resolution for biological samples. Typically, using near-infrared lasers for excitation, CARS or SRS has a lateral resolution on the scale of 300-400 nm. Super-resolution optical imaging to break the diffraction limit has been achieved for fluorescence microscopy,[128–130] but has currently not for CRS. The major reason is that their signal generation principles are disparate. Mechanisms that underpin modern super-resolution optical microscopy, such as ground-state depletion or fluorescent blinking of fluorophores, do not apply to molecular targets of CRS microscopy. Even the samples can be prepared sparse enough to isolate a small group of molecules, sensitivity of current CRS microscopy may fail to resolve the targets without particularly designed enhancement. Currently, the biomolecules that generate strongest CRS signals are lipids due to their high concentration of CH_2 groups. Lipid bilayer membranes can be well resolved using CARS or SRS microscopy.[100] Feasibility to achieve super-resolution CARS microscopy has been discussed.[131,132] Using engineered laser beams such as Bessel beams, CARS imaging with 1.33 times improvement of spatial resolution has been reported.[133] A super-resolution four-wave mixing microscope which can improve the lateral resolution by a factor of 2 was reported by narrowing the excitation volume using a Toraldo-style pupil phase filter.[134] Using photonics nanojets, a CARS microscope with a lateral resolution of 200 nm at 796 nm laser excitation was demonstrated.[135] However, how to beat the diffraction limit of CRS imaging for a resolution below 100 nm still waits for creative solutions.

D. Imaging faster

The emerging of CRS microscopy was triggered by a general need to improve the speed of spontaneous Raman microscopy. Currently, with the help from CARS and SRS, Raman imaging speed can reach the video rate. Further improvement in speed would certainly open more opportunities for the field, however, may touch the plateau of the sensitivity limit. It is highly likely that further enhancing the imaging speed might sacrifice the sensitivity of the system, which may mutilate the technology for applications. CRS imaging is generally not suitable for wide-field excitation and detection due to the requirement of high laser energy density. Meanwhile, we note that proof-of-principle wide-field CARS has been published,[86,136] which offers a route to push the speed to 1000 frames per second. High-speed CRS spectral acquisition has been demonstrated in several ways. The Ideguchi and Goda group developed high-speed Fourier-transform CARS spectroscopy at 20 000 spectra per second.[137] The Polli group demonstrated broadband SRS spectroscopy with single pulses at a speed of 80-kHz rate. With multiplex excitation and a 32-channel TAMP array, an unprecedented speed of 5 μs per SRS spectrum has been achieved by the Cheng group.[62] In this method, the technical limits for spectral acquisition speed are reading speeds of detectors or the sampling rates of data acquisition systems. These high-speed spectral acquisition methods can further promote the speed of hyperspectral CRS imaging. Towards high-speed volumetric imaging, engineered laser beams such as Bessel beams were shown to be helpful.[71,89] To further improve the imaging speed of CRS microscopy, better sensitivity is generally desired.

E. Reducing phototoxicity through the use of a second optical window

Tight laser focusing used in CRS microscopy might introduce phototoxicity to biological systems. Many groups have measured the phototoxicity and photodamage of lasers to samples and determined the safe energy-limit for living samples in CRS imaging.[138–140] CRS microscopy usually deploys near-IR beams for excitation, which largely avoid electronic excitation for most biomolecules. Higher sample damage threshold was found with longer excitation wavelength.[26] Consequently, a possible way to reduce phototoxicity and photodamage in CRS without sacrificing sensitivity is to use longer wavelength for excitation. Combinations of both Er-(~1550 nm) and Yb-(~1040 nm),[120] and Tm-(~2000 nm) and Er-doped[141] fiber laser/amplifier systems were used for CRS microscopy. Laser systems with even longer wavelength might further reduce phototoxicity for CRS imaging.

F. Miniaturization

Most CRS microscopes utilize tight-laser-focusing and high-speed laser scanning for image generation. 2D laser raster scanning is a mature technology for modern fluorescence microscopy, typically achieved by a 2D galvo mirror installed inside a confocal microscope. Although a powerful platform, a CRS microscope implemented this way is bulky and can only study samples prepared on glass slides or animals small enough to be placed on the sample stage. In order to deliver the imaging probes to the subject, efforts have been put into miniaturizing the CRS microscope.

One approach is to build flexible probes by free-space or fiber-based delivery of excitation lasers. The König group integrated CARS imaging into a multiphoton tomograph system to collect optical biopsies for *in vivo* histology.[142] Such a system can operate in a clinical environment and be used

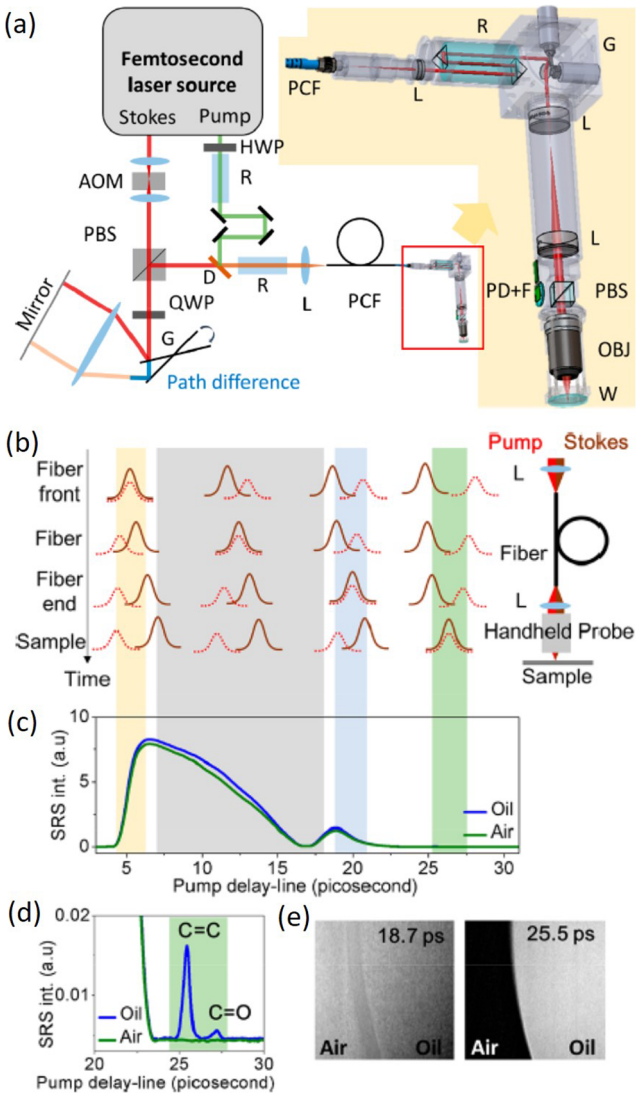

FIG. 6. A hand-held hyperspectral SRS microscope. (a) Design of the optical system and the handheld probe. AOM: acousto-optic modulator; D: dichroic mirror; F: filter; G: galvo mirror; HWP: half-wave plate; L: lens; OBJ: objective; PBS: polarizing beam splitter; PCF: photonics crystal fiber; PD: photodiode; QWP: quarter-wave plate; R: rod (SF-11); W: window. (b) Temporal overlap of the pump and Stokes pulses at the fiber front tip, inside the fiber, at the fiber end tip, and on the sample. (c) Spectral profiles of fiber background and Raman signals of the sample, (d) Zoom-in view of signals in (c). (e) Image of the olive oil/air interface at 18.7 and 25.5 ps pump delay position. Adapted with permission from Liao *et al.*, ACS Photonics **5**(3), 947–954 (2017). Copyright 2017 American Chemical Society.

by briefly trained non-laser experts. Smith *et al.* built a miniaturize multimodal exoscope which can simultaneously collect CARS, second harmonic generation (SHG), and two-photon excitation fluorescence (TPEF) photons in the epi-direction.[143] Liao *et al.* designed a hand-held probe for *in situ* hyperspectral SRS microscopy of cancerous tissue and skin (Fig. 6).[144]

Another more challenging approach is to develop all-fiber-based CRS endoscopic probes, which usually have a diameter of a few millimeters in order to enter the endoscope channels. Multiple groups were engaged to develop miniature fiber endoscopic probes for multiphoton microscopy. Fiber scanning[145–150] or microelectromechanical system (MEMS) scanning[151–154] was used to generate images by miniature fiber probes. Compared to endoscopic probes for TPEF and SHG, CRS probes experience more challenges majorly due to the requirement for delivering two laser beams with a large frequency discrepancy. First, fibers can generate a strong nonlinear signal background for both the CARS and SRS signal detection. Several approaches were used to reduce or separate the fiber background from the CRS signals generated from the sample. The background from the delivery fiber can be largely eliminated by applying optical filters in the probe,[155] or reduced by using cross-polarization propagation of two excitation beams,[156] or separated from the sample signal in time domain (Fig. 6).[144] Second, it is challenging to design miniature lenses to compensate chromatic aberration in a broad frequency range covering the two excitation beams. In addition, optimizing signal collection from the fiber probe is critical to improve the sensitivity of CRS probes. The CARS signal can be generated in the epi-direction, while the SRS signal only follows the input laser beams. The SRS signal collected by the fiber probes is usually from purely sample-scattered or -reflected photons. Therefore, the detector is preferred to be placed close to the sample for signal detection in an SRS endoscope.[157] Notably, SRS imaging can operate under ambient light, which is compatible with clinical applications.

IV. CONCLUSION

Over the past two decades, great efforts have been put to advance CRS microscopy into a powerful and practical tool to quantify chemical compositions in living biological samples. This new imaging modality has infiltrated into numerous applications in both fundamental research and clinical settings, breeding new discoveries in biology and medicine. Although challenges still remain, especially for higher detection sensitivity, CRS microscopy has offered and will continue to provide unprecedented chemical information for scientists and doctors to look into biological functions from a novel angle. The field of CRS microscopy is highly interdisciplinary, which merges physics, chemistry, engineering, biology, and mathematics. Many of the advancements in the field are inextricable to progresses in other fields, such as improved laser technology, better detectors, breakthroughs in chemical engineering, and the development of new data analysis algorithms. New concepts and technologies in other fields will continue to permeate into CRS microscopy and culminate revolutionary changes. From such expectations, we foresee a brilliant future of CRS microscopy to become a staple analytical tool for the interrogation of frontiers and key questions in biological, medical, and material sciences.

ACKNOWLEDGMENTS

The authors acknowledge the support from NIH Grant No. GM118471 and a Science and Engineering Grant from Keck Foundation.

[1] C. V. Raman and K. S. Krishnan, Nature **121**(3048), 501–502 (1928).
[2] C. V. Raman, Proc. Indian Acad. Sci., Sect. A **37**(3), 342–349 (1953).
[3] R. W. Boyd, *Nonlinear Optics* (Academic Press, 2003).
[4] J.-X. Cheng and X. S. Xie, *Coherent Raman Scattering Microscopy* (CRC Press, 2016).
[5] R. Terhune, P. Maker, and C. Savage, Phys. Rev. Lett. **14**(17), 681 (1965).
[6] R. Begley, A. Harvey, and R. L. Byer, Appl. Phys. Lett. **25**(7), 387–390 (1974).
[7] K. Marko and L. Rimai, Opt. Lett. **4**(7), 211–213 (1979).
[8] B. Attal, M. Pealat, and J.-P. Taran, J. Energy **4**(3), 135–141 (1980).
[9] F. Beyrau, A. Datta, T. Seeger, and A. Leipertz, J. Raman Spectrosc. **33**(11-12), 919–924 (2002).
[10] A. Ehn, J. Zhu, X. Li, and J. Kiefer, Appl. Spectrosc. **71**(3), 341–366 (2017).
[11] M. D. Duncan, J. Reintjes, and T. Manuccia, Opt. Lett. **7**(8), 350–352 (1982).
[12] A. Zumbusch, G. R. Holtom, and X. S. Xie, Phys. Rev. Lett. **82**(20), 4142 (1999).

[13] J.-X. Cheng, A. Volkmer, and X. S. Xie, J. Opt. Soc. Am. B **19**(6), 1363–1375 (2002).
[14] C. L. Evans, E. O. Potma, M. Puoris'haag, D. Côté, C. P. Lin, and X. S. Xie, Proc. Natl. Acad. Sci. U. S. A. **102**(46), 16807–16812 (2005).
[15] J.-X. Cheng, L. D. Book, and X. S. Xie, Opt. Lett. **26**(17), 1341–1343 (2001).
[16] J.-x. Cheng, A. Volkmer, L. D. Book, and X. S. Xie, J. Phys. Chem. B **105**(7), 1277–1280 (2001).
[17] F. Ganikhanov, C. L. Evans, B. G. Saar, and X. S. Xie, Opt. Lett. **31**(12), 1872–1874 (2006).
[18] D. L. Marks and S. A. Boppart, Phys. Rev. Lett. **92**(12), 123905 (2004).
[19] Y. Liu, Y. J. Lee, and M. T. Cicerone, Opt. Lett. **34**(9), 1363–1365 (2009).
[20] E. Woodbury and W. Ng, Proc. Inst. Radio Eng. **50**(11), 2347–2348 (1962).
[21] A. Owyoung and E. D. Jones, Opt. Lett. **1**(5), 152–154 (1977).
[22] E. Ploetz, S. Laimgruber, S. Berner, W. Zinth, and P. Gilch, Appl. Phys. B **87**(3), 389–393 (2007).
[23] C. W. Freudiger, W. Min, B. G. Saar, S. Lu, G. R. Holtom, C. He, J. C. Tsai, J. X. Kang, and X. S. Xie, Science **322**(5909), 1857–1861 (2008).
[24] Y. Ozeki, F. Dake, S. i. Kajiyama, K. Fukui, and K. Itoh, Opt. Express **17**(5), 3651–3658 (2009).
[25] P. Nandakumar, A. Kovalev, and A. Volkmer, New J. Phys. **11**(3), 033026 (2009).
[26] D. Zhang, M. N. Slipchenko, and J.-X. Cheng, J. Phys. Chem. Lett. **2**(11), 1248–1253 (2011).
[27] M. N. Slipchenko, T. T. Le, H. Chen, and J.-X. Cheng, J. Phys. Chem. B **113**(21), 7681–7686 (2009).
[28] C. Zhang, D. Zhang, and J.-X. Cheng, Annu. Rev. Biomed. Eng. **17**, 415–445 (2015).
[29] W. Min, C. W. Freudiger, S. Lu, and X. S. Xie, Annu. Rev. Phys. Chem. **62**, 507–530 (2011).
[30] S. Yue, M. N. Slipchenko, and J. X. Cheng, Laser Photonics Rev. **5**(4), 496–512 (2011).
[31] E. O. Potma, C. L. Evans, and X. S. Xie, Opt. Lett. **31**(2), 241–243 (2006).
[32] X. Nan, J.-X. Cheng, and X. S. Xie, J. Lipid Res. **44**(11), 2202–2208 (2003).
[33] H. Wang, Y. Fu, P. Zickmund, R. Shi, and J.-X. Cheng, Biophys. J. **89**(1), 581–591 (2005).
[34] F.-K. Lu, M. Ji, D. Fu, X. Ni, C. W. Freudiger, G. Holtom, and X. S. Xie, Mol. Phys. **110**(15-16), 1927–1932 (2012).
[35] L. Kong, M. Ji, G. R. Holtom, D. Fu, C. W. Freudiger, and X. S. Xie, Opt. Lett. **38**(2), 145–147 (2013).
[36] R. He, Y. Xu, L. Zhang, S. Ma, X. Wang, D. Ye, and M. Ji, Optica **4**(1), 44–47 (2017).
[37] B. Zhang, M. Sun, Y. Yang, L. Chen, X. Zou, T. Yang, Y. Hua, and M. Ji, Biomed. Opt. Express **9**(6), 2604–2613 (2018).
[38] F.-K. Lu, S. Basu, V. Igras, M. P. Hoang, M. Ji, D. Fu, G. R. Holtom, V. A. Neel, C. W. Freudiger, and D. E. Fisher, Proc. Natl. Acad. Sci. U. S. A. **112**(37), 11624–11629 (2015).
[39] C. W. Freudiger, R. Pfannl, D. A. Orringer, B. G. Saar, M. Ji, Q. Zeng, L. Ottoboni, W. Ying, C. Waeber, and J. R. Sims, Lab. Invest. **92**(10), 1492 (2012).
[40] F.-K. Lu, D. Calligaris, O. I. Olubiyi, I. Norton, W. Yang, S. Santagata, X. S. Xie, A. J. Golby, and N. Y. Agar, Cancer Res. **76**(12), 3451–3462 (2016).
[41] T. Hellerer, A. M. Enejder, and A. Zumbusch, Appl. Phys. Lett. **85**(1), 25–27 (2004).
[42] I. Rocha-Mendoza, W. Langbein, and P. Borri, Appl. Phys. Lett. **93**(20), 201103 (2008).
[43] J.-x. Cheng, A. Volkmer, L. D. Book, and X. S. Xie, J. Phys. Chem. B **106**(34), 8493–8498 (2002).
[44] M. Müller and J. M. Schins, J. Phys. Chem. B **106**(14), 3715–3723 (2002).
[45] R. Selm, M. Winterhalder, A. Zumbusch, G. Krauss, T. Hanke, A. Sell, and A. Leitenstorfer, Opt. Lett. **35**(19), 3282–3284 (2010).
[46] V. Kumar, R. Osellame, R. Ramponi, G. Cerullo, and M. Marangoni, Opt. Express **19**(16), 15143–15148 (2011).
[47] I. Pope, W. Langbein, P. Watson, and P. Borri, Opt. Express **21**(6), 7096–7106 (2013).
[48] T. W. Kee and M. T. Cicerone, Opt. Lett. **29**(23), 2701–2703 (2004).
[49] B. von Vacano, L. Meyer, and M. Motzkus, J. Raman Spectrosc. **38**(7), 916–926 (2007).
[50] A. F. Pegoraro, A. Ridsdale, D. J. Moffatt, Y. Jia, J. P. Pezacki, and A. Stolow, Opt. Express **17**(4), 2984–2996 (2009).
[51] C. H. Camp, Jr., Y. J. Lee, J. M. Heddleston, C. M. Hartshorn, A. R. H. Walker, J. N. Rich, J. D. Lathia, and M. T. Cicerone, Nat. Photonics **8**(8), 627–634 (2014).
[52] Y. Ozeki, W. Umemura, Y. Otsuka, S. Satoh, H. Hashimoto, K. Sumimura, N. Nishizawa, K. Fukui, and K. Itoh, Nat. Photonics **6**(12), 845–851 (2012).
[53] P. Wang, J. Li, P. Wang, C. R. Hu, D. Zhang, M. Sturek, and J. X. Cheng, Angew. Chem., Int. Ed. **52**(49), 13042–13046 (2013).
[54] E. R. Andresen, P. Berto, and H. Rigneault, Opt. Lett. **36**(13), 2387–2389 (2011).
[55] D. Fu, G. Holtom, C. Freudiger, X. Zhang, and X. S. Xie, J. Phys. Chem. B **117**(16), 4634–4640 (2013).
[56] R. He, Z. Liu, Y. Xu, W. Huang, H. Ma, and M. Ji, Opt. Lett. **42**(4), 659–662 (2017).
[57] C.-S. Liao, K.-C. Huang, W. Hong, A. J. Chen, C. Karanja, P. Wang, G. Eakins, and J.-X. Cheng, Optica **3**(12), 1377–1380 (2016).
[58] H. Lin, C.-S. Liao, P. Wang, N. Kong, and J.-X. Cheng, Light Sci. Appl. **7**, 17179 (2018).
[59] W. Rock, M. Bonn, and S. H. Parekh, Opt. Express **21**(13), 15113–15120 (2013).
[60] K. Seto, Y. Okuda, E. Tokunaga, and T. Kobayashi, Rev. Sci. Instrum. **84**(8), 083705 (2013).
[61] C.-S. Liao, M. N. Slipchenko, P. Wang, J. Li, S.-Y. Lee, R. A. Oglesbee, and J.-X. Cheng, Light Sci. Appl. **4**(3), e265 (2015).
[62] C. Zhang, K.-C. Huang, B. Rajwa, J. Li, S. Yang, H. Lin, C.-s. Liao, G. Eakins, S. Kuang, and V. Patsekin, Optica **4**(1), 103–109 (2017).
[63] C.-S. Liao, P. Wang, P. Wang, J. Li, H. J. Lee, G. Eakins, and J.-X. Cheng, Sci. Adv. **1**(9), e1500738 (2015).
[64] D. Zhang, P. Wang, M. N. Slipchenko, D. Ben-Amotz, A. M. Weiner, and J.-X. Cheng, Anal. Chem. **85**(1), 98–106 (2012).
[65] A. Khmaladze, J. Jasensky, E. Price, C. Zhang, A. Boughton, X. Han, E. Seeley, X. Liu, M. M. B. Holl, and Z. Chen, Appl. Spectrosc. **68**(10), 1116–1122 (2014).
[66] F. Masia, A. Glen, P. Stephens, P. Borri, and W. Langbein, Anal. Chem. **85**(22), 10820–10828 (2013).
[67] C. Di Napoli, I. Pope, F. Masia, P. Watson, W. Langbein, and P. Borri, Biomed. Opt. Express **5**(5), 1378–1390 (2014).
[68] F. Masia, A. Karuna, P. Borri, and W. Langbein, J. Raman Spectrosc. **46**(8), 727–734 (2015).

[69] C. Di Napoli, I. Pope, F. Masia, W. Langbein, P. Watson, and P. Borri, Anal. Chem. **88**(7), 3677–3685 (2016).
[70] F. Masia, P. Borri, and W. Langbein, Opt. Express **22**(4), 4021–4028 (2014).
[71] F. Masia, I. Pope, P. Watson, W. Langbein, and P. Borri, Anal. Chem. **90**(6), 3775–3785 (2018).
[72] E. M. Vartiainen, H. A. Rinia, M. Müller, and M. Bonn, Opt. Express **14**(8), 3622–3630 (2006).
[73] H. A. Rinia, M. Bonn, M. Müller, and E. M. Vartiainen, ChemPhysChem **8**(2), 279–287 (2007).
[74] M. Okuno, H. Kano, P. Leproux, V. Couderc, J. P. Day, M. Bonn, and H. o. Hamaguchi, Angew. Chem., Int. Ed. **49**(38), 6773–6777 (2010).
[75] D. Fu, J. Zhou, W. S. Zhu, P. W. Manley, Y. K. Wang, T. Hood, A. Wylie, and X. S. Xie, Nat. Chem. **6**(7), 614 (2014).
[76] S. Yue, J. Li, S.-Y. Lee, H. J. Lee, T. Shao, B. Song, L. Cheng, T. A. Masterson, X. Liu, and T. L. Ratliff, Cell Metab. **19**(3), 393–406 (2014).
[77] J. Li, S. Condello, J. Thomes-Pepin, X. Ma, Y. Xia, T. D. Hurley, D. Matei, and J.-X. Cheng, Cell Stem Cell **20**(3), 303–314 (2017).
[78] M. Jurna, J. P. Korterik, C. Otto, and H. L. Offerhaus, Opt. Express **15**(23), 15207–15213 (2007).
[79] W. Hong, C. S. Liao, H. Zhao, W. Younis, Y. Zhang, M. N. Seleem, and J. X. Cheng, ChemistrySelect **1**(3), 513–517 (2016).
[80] S. Yampolsky, D. A. Fishman, S. Dey, E. Hulkko, M. Banik, E. O. Potma, and V. A. Apkarian, Nat. Photonics **8**(8), 650–656 (2014).
[81] I. Rajapaksa and H. Kumar Wickramasinghe, Appl. Phys. Lett. **99**(16), 161103 (2011).
[82] J. Jahng, D. A. Fishman, S. Park, D. B. Nowak, W. A. Morrison, H. K. Wickramasinghe, and E. O. Potma, Acc. Chem. Res. **48**(10), 2671–2679 (2015).
[83] H. J. Lee, W. Zhang, D. Zhang, Y. Yang, B. Liu, E. L. Barker, K. K. Buhman, L. V. Slipchenko, M. Dai, and J.-X. Cheng, Sci. Rep. **5**, 7930 (2015).
[84] L. Wei, Z. Chen, L. Shi, R. Long, A. V. Anzalone, L. Zhang, F. Hu, R. Yuste, V. W. Cornish, and W. Min, Nature **544**(7651), 465–470 (2017).
[85] C.-S. Liao, J. H. Choi, D. Zhang, S. H. Chan, and J.-X. Cheng, J. Phys. Chem. C **119**(33), 19397–19403 (2015).
[86] C. Heinrich, S. Bernet, and M. Ritsch-Marte, Appl. Phys. Lett. **84**(5), 816–818 (2004).
[87] I. Toytman, K. Cohn, T. Smith, D. Simanovskii, and D. Palanker, Opt. Lett. **32**(13), 1941–1943 (2007).
[88] A. S. Duarte, C. Schnedermann, and P. Kukura, Sci. Rep. **6**, 37516 (2016).
[89] X. Chen, C. Zhang, P. Lin, K.-C. Huang, J. Liang, J. Tian, and J.-X. Cheng, Nat. Commun. **8**, 15117 (2017).
[90] L. Wei, F. Hu, Y. Shen, Z. Chen, Y. Yu, C.-C. Lin, M. C. Wang, and W. Min, Nat. Methods **11**(4), 410–412 (2014).
[91] S. Hong, T. Chen, Y. Zhu, A. Li, Y. Huang, and X. Chen, Angew. Chem., Int. Ed. **53**(23), 5827–5831 (2014).
[92] L. Wei, F. Hu, Z. Chen, Y. Shen, L. Zhang, and W. Min, Acc. Chem. Res. **49**(8), 1494–1502 (2016).
[93] Z. Zhao, Y. Shen, F. Hu, and W. Min, Analyst **142**(21), 4018–4029 (2017).
[94] L. Wei, Y. Yu, Y. Shen, M. C. Wang, and W. Min, Proc. Natl. Acad. Sci. U. S. A. **110**(28), 11226–11231 (2013).
[95] L. Wei, Y. Shen, F. Xu, F. Hu, J. K. Harrington, K. L. Targoff, and W. Min, ACS Chem. Biol. **10**(3), 901–908 (2015).
[96] F. Hu, C. Zeng, R. Long, Y. Miao, L. Wei, Q. Xu, and W. Min, Nat. Methods **15**(3), 194–200 (2018).
[97] L. Li, H. Wang, and J.-X. Cheng, Biophys. J. **89**(5), 3480–3490 (2005).
[98] Y. Shen, F. Xu, L. Wei, F. Hu, and W. Min, Angew. Chem., Int. Ed. **53**(22), 5596–5599 (2014).
[99] J.-X. Cheng, S. Pautot, D. A. Weitz, and X. S. Xie, Proc. Natl. Acad. Sci. U. S. A. **100**(17), 9826–9830 (2003).
[100] E. O. Potma and X. S. Xie, J. Raman Spectrosc. **34**(9), 642–650 (2003).
[101] H. A. Rinia, G. W. Wurpel, and M. Müller, *Methods in Membrane Lipids* (Springer, 2007), pp. 45–61.
[102] F. Lu, W. Zheng, and Z. Huang, Opt. Lett. **34**(12), 1870–1872 (2009).
[103] G. de Vito, A. Bifone, and V. Piazza, Opt. Express **20**(28), 29369–29377 (2012).
[104] M. Hofer, N. K. Balla, and S. Brasselet, Optica **4**(7), 795–801 (2017).
[105] C. Cleff, A. Gasecka, P. Ferrand, H. Rigneault, S. Brasselet, and J. Duboisset, Nat. Commun. **7**, 11562 (2016).
[106] H.-W. Wang, N. Bao, T. T. Le, C. Lu, and J.-X. Cheng, Opt. Express **16**(8), 5782–5789 (2008).
[107] C. H. Camp, Jr., S. Yegnanarayanan, A. A. Eftekhar, H. Sridhar, and A. Adibi, Opt. Express **17**(25), 22879–22889 (2009).
[108] C. H. Camp, Jr., S. Yegnanarayanan, A. A. Eftekhar, and A. Adibi, Opt. Lett. **36**(12), 2309–2311 (2011).
[109] C. L. Evans, X. Xu, S. Kesari, X. S. Xie, S. T. Wong, and G. S. Young, Opt. Express **15**(19), 12076–12087 (2007).
[110] O. Uckermann, R. Galli, S. Tamosaityte, E. Leipnitz, K. D. Geiger, G. Schackert, E. Koch, G. Steiner, and M. Kirsch, PLoS One **9**(9), e107115 (2014).
[111] C. Pohling, T. Bocklitz, A. S. Duarte, C. Emmanuello, M. S. Ishikawa, B. Dietzeck, T. Buckup, O. Uckermann, G. Schackert, and M. Kirsch, J. Biomed. Opt. **22**(6), 066005 (2017).
[112] M. Ji, D. A. Orringer, C. W. Freudiger, S. Ramkissoon, X. Liu, D. Lau, A. J. Golby, I. Norton, M. Hayashi, and N. Y. Agar, Sci. Transl. Med. **5**(201), 201ra119 (2013).
[113] M. Ji, S. Lewis, S. Camelo-Piragua, S. H. Ramkissoon, M. Snuderl, S. Venneti, A. Fisher-Hubbard, M. Garrard, D. Fu, and A. C. Wang, Sci. Transl. Med. **7**(309), 309ra163 (2015).
[114] D. A. Orringer, B. Pandian, Y. S. Niknafs, T. C. Hollon, J. Boyle, S. Lewis, M. Garrard, S. L. Hervey-Jumper, H. J. Garton, and C. O. Maher, Nat. Biomed. Eng. **1**(2), 0027 (2017).
[115] E. R. Andresen, C. K. Nielsen, J. Thøgersen, and S. R. Keiding, Opt. Express **15**(8), 4848–4856 (2007).
[116] A. F. Pegoraro, A. Ridsdale, D. J. Moffatt, J. P. Pezacki, B. K. Thomas, L. Fu, L. Dong, M. E. Fermann, and A. Stolow, Opt. Express **17**(23), 20700–20706 (2009).
[117] K. Kieu, B. G. Saar, G. R. Holtom, X. S. Xie, and F. W. Wise, Opt. Lett. **34**(13), 2051–2053 (2009).
[118] M. Baumgartl, T. Gottschall, J. Abreu-Afonso, A. Díez, T. Meyer, B. Dietzek, M. Rothhardt, J. Popp, J. Limpert, and A. Tünnermann, Opt. Express **20**(19), 21010–21018 (2012).
[119] C. Xu and F. Wise, Nat. Photonics **7**(11), 875–882 (2013).
[120] C. W. Freudiger, W. Yang, G. R. Holtom, N. Peyghambarian, X. S. Xie, and K. Q. Kieu, Nat. Photonics **8**(2), 153–159 (2014).
[121] D. Zhang, C. Li, C. Zhang, M. N. Slipchenko, G. Eakins, and J.-X. Cheng, Sci. Adv. **2**(9), e1600521 (2016).

[122] A. J. Traverso, B. Hokr, Z. Yi, L. Yuan, S. Yamaguchi, M. O. Scully, and V. V. Yakovlev, Phys. Rev. Lett. **120**(6), 063602 (2018).
[123] N. Ji, D. E. Milkie, and E. Betzig, Nat. Methods **7**(2), 141–147 (2010).
[124] V. V. Tuchin, *Tissue Optics: Light Scattering Methods and Instruments for Medical Diagnosis* (SPIE Press, 2007).
[125] F. O. Fahrbach, P. Simon, and A. Rohrbach, Nat. Photonics **4**(11), 780–785 (2010).
[126] S. B. Purnapatra, S. Bera, and P. P. Mondal, Sci. Rep. **2**, 692 (2012).
[127] F. O. Fahrbach, V. Gurchenkov, K. Alessandri, P. Nassoy, and A. Rohrbach, Opt. Express **21**(11), 13824–13839 (2013).
[128] S. W. Hell and J. Wichmann, Opt. Lett. **19**(11), 780–782 (1994).
[129] E. Betzig, G. H. Patterson, R. Sougrat, O. W. Lindwasser, S. Olenych, J. S. Bonifacino, M. W. Davidson, J. Lippincott-Schwartz, and H. F. Hess, Science **313**(5793), 1642–1645 (2006).
[130] B. Huang, M. Bates, and X. Zhuang, Annu. Rev. Biochem. **78**, 993–1016 (2009).
[131] W. P. Beeker, C. J. Lee, K. J. Boller, P. Groß, C. Cleff, C. Fallnich, H. L. Offerhaus, and J. L. Herek, J. Raman Spectrosc. **42**(10), 1854–1858 (2011).
[132] L. Gong and H. Wang, Phys. Rev. A **90**(1), 013818 (2014).
[133] S. Heuke, F. B. Legesse, D. Akimov, U. Hübner, J. Dellith, M. Schmitt, and J. Popp, J. Opt. Soc. Am. B **32**(9), 1773–1779 (2015).
[134] H. Kim, G. W. Bryant, and S. J. Stranick, Opt. Express **20**(6), 6042–6051 (2012).
[135] P. K. Upputuri, Z. Wu, L. Gong, C. K. Ong, and H. Wang, Opt. Express **22**(11), 12890–12899 (2014).
[136] C. Heinrich, A. Hofer, A. Ritsch, C. Ciardi, S. Bernet, and M. Ritsch-Marte, Opt. Express **16**(4), 2699–2708 (2008).
[137] K. Hashimoto, M. Takahashi, T. Ideguchi, and K. Goda, Sci. Rep. **6**, 21036 (2016).
[138] X. Nan, E. O. Potma, and X. S. Xie, Biophys. J. **91**(2), 728–735 (2006).
[139] Y. Fu, H. Wang, R. Shi, and J.-X. Cheng, Opt. Express **14**(9), 3942–3951 (2006).
[140] H. Wang, Y. Fu, and J.-X. Cheng, J. Opt. Soc. Am. B **24**(3), 544–552 (2007).
[141] N. Coluccelli, V. Kumar, M. Cassinerio, G. Galzerano, M. Marangoni, and G. Cerullo, Opt. Lett. **39**(11), 3090–3093 (2014).
[142] M. Weinigel, H. Breunig, M. Kellner-Höfer, R. Bückle, M. Darvin, M. Klemp, J. Lademann, and K. König, Laser Phys. Lett. **11**(5), 055601 (2014).
[143] B. Smith, M. Naji, S. Murugkar, E. Alarcon, C. Brideau, P. Stys, and H. Anis, Opt. Express **21**(14), 17161–17175 (2013).
[144] C.-S. Liao, P. Wang, C. Y. Huang, P. Lin, G. Eakins, R. T. Bentley, R. Liang, and J.-X. Cheng, ACS Photonics **5**(3), 947–954 (2017).
[145] F. Helmchen, M. S. Fee, D. W. Tank, and W. Denk, Neuron **31**(6), 903–912 (2001).
[146] M. T. Myaing, D. J. MacDonald, and X. Li, Opt. Lett. **31**(8), 1076–1078 (2006).
[147] C. J. Engelbrecht, R. S. Johnston, E. J. Seibel, and F. Helmchen, Opt. Express **16**(8), 5556–5564 (2008).
[148] D. R. Rivera, C. M. Brown, D. G. Ouzounov, I. Pavlova, D. Kobat, W. W. Webb, and C. Xu, Proc. Natl. Acad. Sci. U. S. A. **108**(43), 17598–17603 (2011).
[149] Y. Zhang, M. L. Akins, K. Murari, J. Xi, M.-J. Li, K. Luby-Phelps, M. Mahendroo, and X. Li, Proc. Natl. Acad. Sci. U. S. A. **109**(32), 12878–12883 (2012).
[150] K. Hwang, Y.-H. Seo, and K.-H. Jeong, Micro Nano Syst. Lett. **5**(1), 1 (2017).
[151] C. L. Hoy, N. J. Durr, P. Chen, W. Piyawattanametha, H. Ra, O. Solgaard, and A. Ben-Yakar, Opt. Express **16**(13), 9996–10005 (2008).
[152] T.-M. Liu, M.-C. Chan, I.-H. Chen, S.-H. Chia, and C.-K. Sun, Opt. Express **16**(14), 10501–10506 (2008).
[153] S. Tang, W. Jung, D. T. McCormick, T. Xie, J. Su, Y.-C. Ahn, B. J. Tromberg, and Z. Chen, J. Biomed. Opt. **14**(3), 034005 (2009).
[154] Z. Qiu and W. Piyawattanamatha, Micromachines **8**(7), 210 (2017).
[155] A. Lukic, S. Dochow, H. Bae, G. Matz, I. Latka, B. Messerschmidt, M. Schmitt, and J. Popp, Optica **4**(5), 496–501 (2017).
[156] Z. Wang, Y. Liu, L. Gao, Y. Chen, P. Luo, K. K. Wong, and S. T. Wong, Opt. Lett. **36**(15), 2967–2969 (2011).
[157] B. G. Saar, R. S. Johnston, C. W. Freudiger, X. S. Xie, and E. J. Seibel, Opt. Lett. **36**(13), 2396–2398 (2011).